On the Equivalence of Gas and Liquid Leak Flow Rates for Application to Propulsion and Propellant Transfer Systems

Max Kandula[1], Brian M. Nufer[2]
NASA Kennedy Space Center, Florida 32899

The equivalence of leak rates for gas flow and liquid flow through an arbitrary small leak size in pressurized systems has been investigated theoretically and experimentally. Measurements were taken for gaseous helium (GHe) rates and water flow issuing from the same leak configuration. The predictions for the correlation of GHe leak rates to water leak rates have been satisfactorily compared with present test data and those of other investigators over a wide range leak flow rates (many orders of magnitude) corresponding to a wide range of leak sizes (0.1 μm to 0.1 mm). The results show that at extremely small leak sizes (sub-micron range), the effects of Knudsen number in the free-molecular regime (rarefied gases) become important. By a proper scaling procedure, the measured flow rate for water could be applied to equivalent propellant leaks in flight operations. In the present tests the micro-channel range of the leak size is satisfactorily simulated by repeatable precision set needle position valve. Test results show that in general the theoretical model predicts the data reasonably well for GHe flow rates in the range of 0.001 to 1 sccs. Outside this range of GHe flow rates some adjustments (improvements) to the analytical model are required along with further testing.

Nomenclature

A	=	cross-sectional area
c_s	=	speed of sound
c_p	=	specific heat at constant pressure
C_d	=	discharge coefficient
d	=	tube internal diameter
H	=	microchannel height
Kn	=	Knudsen number, λ / L_c
L	=	effective length of the leak
L_c	=	characteristic length (size) of the leak
m	=	mass
$\dot{m}$	=	mass flow rate
p	=	pressure
q	=	volumetric liquid flow rate
Q	=	normalized volume flux per unit width of channel
R	=	gas constant
Re	=	Reynolds number
t	=	time
T	=	temperature
t	=	time, also tube wall thickness
V	=	volume
W	=	microchannel width
γ	=	specific heat ratio
λ	=	mean free path of molecules
μ	=	dynamic viscosity of fluid

[1] Technical Fellow, KBR, Mail Stop LASSO-001, Associate Fellow, AIAA
[2] OSAM-1 Propellant Transfer Assembly Lead, Explorations Payloads Branch, Mail-Stop NE-L5.

ρ = density of fluid

Subscripts

cr = critical
g = gas
l = liquid
0 = initial state

I. Introduction

Prior to flowing propellant from a Space Vehicle (SV) into the client spacecraft with regard to in-space propellant transfer applications, an on-orbit leak test of the client interface using gaseous helium (GHe) is required to verify the integrity of the interface seals. The ability to accurately characterize a propellant leak/flow rate correlated from a measured helium leak/flow rate for a given system is important in flight applications.

There are many factors that can impact a leak rate. According to the following quote by Blair and Senear[1]: *"Flow rate through a leak is controlled by a great many parameters. Among the most important of these are the geometry of the leak path, including its length, cross-sectional area, and its tortuosity, the pressure differential across the leak which acts as a driving force, the phase of the leaking fluid (e.g. gaseous or liquid) not only on both sides of the leak but also within the leak, and the type of flow at every position within the leak."* This quote summarizes a wide-range of factors that could explain potential discrepancies between various measured leaks in flight, differences between leaks in a flight system and a flight-like ground test setup, along with differences amongst separate ground setups.

The type of flow in the leak path could be molecular (Knudsen flow), laminar, or turbulent, depending on the leak cross-sectional area which could vary over several orders of magnitude for a given system pressure. According to the hypothesis proposed by Blair and Senear[1] that the gas flow type in the vacuum of space will be molecular at lowest flow rates ($<10^{-5}$ sccs helium), laminar at the intermediate flow rates (10^{-1} to 10^{-6} sccs helium), and turbulent at the higher flow rates ($>10^{-2}$ sccs helium) with noted overlaps. It is expected that the leak outlet pressure differences (variations) between the ground setup (ambient) and the flight condition (vacuum) will not be appreciable since the system pressures of interest are considerably large relative to the ambient pressures (atmospheric pressure in the ground setup or vacuum pressure in the flight case).

Typically, the pressure decay during on-orbit client interface helium leak testing enables the ground operators to estimate the leak size and the corresponding initial helium leak flow rate with a known system pressure, temperature, and volume. With the knowledge of the estimated helium leak rate, it is possible to predict the corresponding propellant leak rate for the same system parameters if the equivalence between the gaseous leak rate and propellant leak rate can be deduced from an established (validated) theoretical model with sufficient accuracy. Water is typically used as a simulant or substitute fluid for propellants (typically hypergols) for ground leak check verification.

In the present work, correlation of a helium flow/leak rate to an equivalent water flow/leak rate in flight for an arbitrary leak size has been investigated analytically and experimentally. The analysis takes into account various flow regimes. Ground test data performed are presented in an effort to correlate helium flow rates to liquid demineralized water flow rates within the measurable leak detection range of a given system. The liquid water flow rate can be scaled to determine the propellant flow rates for application to flight leak estimates.

II. Analysis

Figure 1 shows a schematic of the gas or liquid leak (discharge) from a tank of volume V through an orifice or a nozzle of diameter d. The tank volume is constant, while the mass in the tank varies as the gas is discharged from the tank. The quantity p denotes the pressure, T the temperature, ρ the density, and $\dot{m}$ is the discharge mass flow rate.

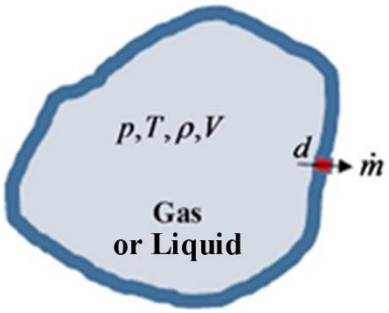


Fig. 1 Schematic of a gas or liquid leak.

A schematic of an arbitrarily sized leak path is presented in **Fig. 2**. In general, the characteristics of the leak governing the leak flow rate include the smallest leak diameter in the hole path (d), the path length of the hole (L) through the component under consideration, surface tension, and the surface finish (roughness) of the hole (leak)[2].

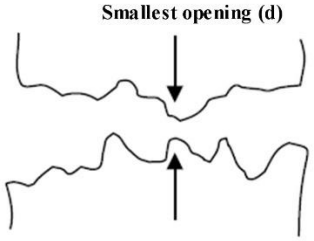


Fig. 2 Representation of an arbitrary leak path.

A. Gaseous Leak Flow

Choked Mass Flow Rate

It is assumed in the present analysis that the gas leak flow is predominantly governed by choked flow in view of the very small size of the leak. Under such circumstances, the gas flow rate through the orifice is considered independent of the length of the passage for moderate passage lengths. Thus, the mass flow rate through the leak orifice for choked flow (sonic flow) for an ideal gas is expressed by the well-known relationship (Shapiro[3])

$$\dot{m} = C_d A_t \sqrt{\frac{\gamma}{R}\left(\frac{2}{\gamma+1}\right)^{\frac{\gamma+1}{\gamma-1}}} \frac{p_1}{\sqrt{T_1}}, \qquad p_2 \le p_{\text{cr}} \text{ (choked flow of gas)} \tag{1a}$$

where the critical pressure p_{cr} is given by

$$\frac{p_{\text{cr}}}{p_1} = \left(\frac{2}{\gamma+1}\right)^{\frac{\gamma}{\gamma-1}} \tag{1b}$$

In the preceding equations, A is the orifice cross sectional area, A_t is the tube cross sectional area, p_1 is the upstream pressure, p_2 is the downstream pressure, T is the gas temperature upstream of the orifice, γ is the specific heat ratio, and C_d is the discharge coefficient. Eq. (1) is based on isentropic expansion of gas through the nozzle/orifice, with non-isentropic effects handled by the introduction of the discharge coefficient C_d .

Since the flow regime could range from continuum to free molecular, depending on the leak diameter which influences the mean free path, appropriate corrections for the discharge coefficient C_d is required.

Discharge Coefficient in the Continuum Regime

The coefficient C_d accounts for the effect of flow losses through friction and vena contracta. For a smooth nozzle, the discharge coefficient is around unity, while for a sharp-edged orifice it is about 0.6, which represents the inviscid incompressible limit. Strictly speaking, the discharge coefficient C_d is a function of the pressure ratio across the orifice and the orifice Reynolds number (Kandula et al.[4]). Thus,

$$C_d = C_d\left(p_r, \mathrm{Re}_d\right) \tag{2a}$$

where

$$p_r = p_2 / p_1 \tag{2b}$$

and Re_d is the orifice Reynolds number based on orifice diameter. The effects of pressure ratio and Reynolds number have been incorporated accordingly.

The variable discharge coefficient is expressed by

$$C_d = C_0\, f_1\left(p_r\right) f_2\left(\mathrm{Re}_d\right), \quad C_0 = 1/0.6 \tag{3a}$$

where

$$f_1\left(p_r\right) = 0.8645 + 0.013088\, p_r - 0.72747\, pr^2 + 0.45159\, pr^3 \tag{3b}$$

$$f_2\left(\mathrm{Re}_d\right) = \begin{cases} 0.1373\,\mathrm{Re}_d^{0.5} \quad (\mathrm{Re}_d < 12) \\ 1.118 - 0.8873\ln\mathrm{Re}_d + 0.3953\left(\ln\mathrm{Re}_d\right)^2 - 0.07081\left(\ln\mathrm{Re}_d\right)^3 \\ +0.005551\left(\ln\mathrm{Re}_d\right)^4 - 0.0001581\left(\ln\mathrm{Re}_d\right)^5 \quad (12 < \mathrm{Re}_d < 5000) \\ 0.59 \quad (\mathrm{Re}_d \geq 5000) \end{cases} \tag{3c}$$

The pressure-ratio correction factor f_1 is obtained from a curve-fit (cubic relation) of the theory of Bragg[5] for C_d vs. pressure ratio. Since the discharge coefficient is very weakly dependent on the specific heat ratio, the data and the curve-fit for C_d air with $\gamma = 1.4$ is expected to satisfactorily apply for helium with $\gamma = 1.67$.

The low-Reynolds number correction factor f_2 is obtained from the Wang et al.[6] based on CFD simulations for various gases (helium, air, hydrogen, and argon), and experimental data due to Tuve and Sprenkle[7] for viscous liquids. At high Reynolds number, the discharge coefficient becomes nearly independent of Reynolds number, and approaches the inviscid incompressible limit. As the Reynolds number decreases, viscous forces become predominant over the inertia forces, and the discharge coefficient decreases. At a Reynolds number of 0.1, the value of C_d reduces to 0.05.

Discharge Coefficient in the Non-Continuum Regimes

In the slip-flow regime (departure from the continuum flow), characteristic of gas flow in microchannels (microleaks), the assumption of continuum flow breaks down and the discharge coefficient depends additionally on the Knudsen number:

$$C_d = C_d\left(p_r, \mathrm{Re}_d, Kn\right) \tag{4a}$$

where Kn is defined by

$$Kn = \lambda / L_c \tag{4b}$$

where λ stands for the mean free path of molecules, and L_c is the characteristic length of the leak (taken here as the equivalent diameter of the leak in view of the orifice choked flow assumption). According to the kinetic theory of gases (Vincenti and Kruger[8]), the mean free path for a gas is expressed by

$$\lambda = \frac{kT}{\sqrt{2}\pi p d_m^2} \tag{4c}$$

where k is the Boltzmann constant (1.3806×10^{-23} m^2.kg.s^{-2}.K^{-1}), T the absolute temperature (K), d_m the molecular diameter, and p the absolute static pressure. The quantity πd_m^2 represents the effective cross-sectional area for collision between molecules. For GHe at 0 deg C, the value of the mean free path is known to be (from Peifer Vacuum)

$$\lambda p = 17.5 \times 10^{-3} \text{ m.Pa} \tag{5}$$

The type of flow regime depends on the Knudsen number (Agrawal[9]). Continuum flow is characterized by $Kn \to 0$. Slip flow is characterized by $0.001 < Kn < 0.1$, transition flow by $0.1 < Kn < 10$, and free molecule flow by $Kn > 10$ (**Fig. 3**).

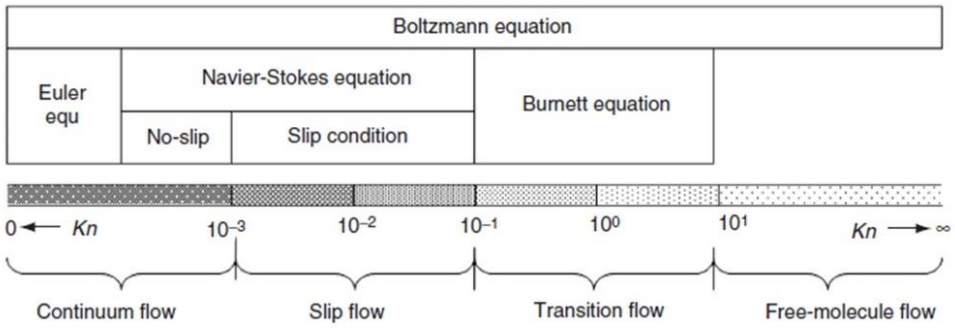


Fig. 3 Flow regimes in terms of Knudsen number (from Agrawal[9]).

Thus, for the slip-flow regime, the orifice discharge coefficient is determined form the relation

$$C_d = C_0 \, f_1(p_r) \, f_2(\mathrm{Re}_d) \, f_3(Kn), \quad C_0 = 1/0.6 \tag{6}$$

where $f_3(Kn)$ is the correction factor to the discharge coefficient in the slip-flow regime (deviation from the continuum theory), which is evaluated as follows.

Figure 4 shows the fully-developed volumetric laminar gas flow rates in a straight microchannel (of uniform cross section) determined from experiments and from various theories (Dongari et al.[10]), as reviewed by Agrawal[9]. For a microchannel of height H the normalized volume flux per unit depth of the channel Q is given by

$$Q = \frac{-\rho c_s \int_0^H U dy}{H^2 (dp/dz)} \tag{7}$$

where ρ is the density, dp/dz is the axial pressure gradient, and c_s is the speed of sound. The volumetric flow rate first decreases with an increase in Knudsen number, reaches a minimum inflection point, then begins to increase.

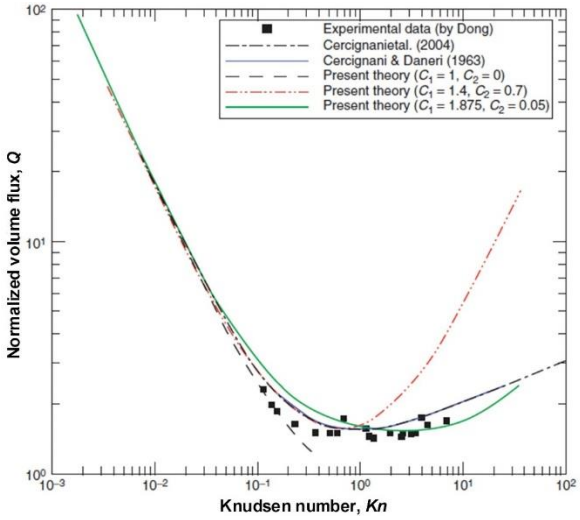


Fig. 4 Dimensionless gas volumetric flow rate vs. Knudsen number in a channel.

The preceding results for the volumetric flow rate in a microchannel cannot be directly applied to the present leak analysis, where the leak path is tortuous, and the gas flow is modeled as an orifice flow under choked conditions. However, in order to introduce the effects of slip on the discharge coefficient of the orifice, we subscribe to an assumption the slip-flow effects in an orifice are likely similar to that observed in a straight microchannel. Thus, the correction coefficient $f_3(Kn)$ for the discharge coefficient in Eq. (6) is approximated by

$$f_3(K_n) = \frac{Q(Kn)}{Q(Kn \to 0)} \tag{8}$$

where $Q(Kn)$ is given in **Fig. 4**. Note that in the present calculations, the Knudsen number is evaluated based on the average pressure p_a (between the supply pressure and the ambient pressure). This average pressure enters only the Knudsen number, which is dimensionless, and not in the mass flow rate relation (1a), unlike in the analysis of Blair and Senear[1].

The discharge coefficient and thus the gas flow rate in the slip flow regime accordingly decreases relative to the continuum flow. **Fig. 5** shows the normalized gas volumetric flow rate (relative to continuum flow), $f_3(Kn)$, as a function of Knudsen number, as adopted from Dongari et al.[10] and Agrawal[9]. It is seen that the normalized volumetric flow rate decreases from unity to about 0.01 at the end of the slip-flow regime ($Kn = 0.1$).

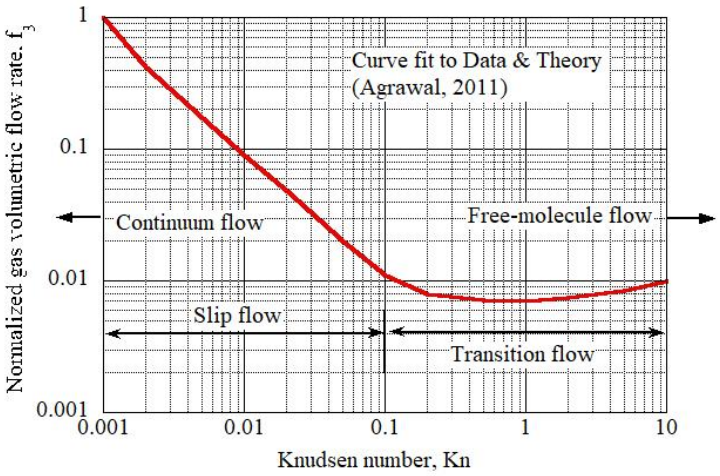


Fig. 5 Normalized volumetric flow rate as a function of Knudsen number.

B. Liquid Leak Flow

From the theory of fully developed laminar flow of liquids, the Poiseuille law yields the volumetric liquid flow rate as (Shames[11]).

$$q = \frac{\pi d^4 \left(p_1 - p_2 \right)}{128 \mu L} \tag{9}$$

where d is the tube diameter, L is the *effective length of the leak path* (tube), and μ is the dynamic viscosity of the liquid. From the initial pressure decay measurements, we can estimate the leak size d. Considering this value of d, and knowing the expected leak length for the liquid flow, it is possible to determine the leak flow rate of the liquid for the given leak size.

Experimental data show that the pressure drop in microchannels can be described by conventional correlations. There was no indication of appreciable deviation from the Navier-Stokes flow theory for rectangular microchannels. Data by Hrnjak and Tu[12] for rectangular microchannels covering a hydraulic diameter range of $69.5 \geq d_H \leq 304.7\,\mu$m and a Reynolds number range of $112 \leq \mathrm{Re} \leq 9180$ confirm this behavior. See **Fig. 6** for the friction factor data for a channel of $69\,\mu$m diameter and an aspect ratio of 0.09 (H, W refer to the height and width respectively).

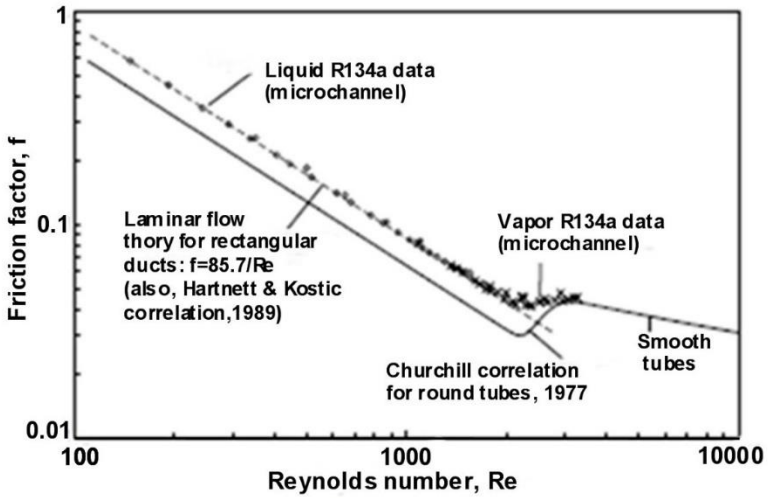


Fig. 6 Data for friction factor for liquid flow through a microscale rectangular duct ($d_H = 69\,\mu$m, $H/W = 0.09$).

In view of the forgoing considerations, Poiseuille law for laminar flow of a liquid, as given by Eq. (9), is considered to be valid for describing the liquid leak flow rates.

C. Equivalence Between Gas and Liquid Leak Flow

From the data on the leak rates measured using helium pressure decay and the theoretical model developed for the pressure decay (Kandula et al.[4]), it is possible to estimate the equivalent liquid flow rates.

III. Test Setup

A. Water Leak Flow Test Setup

Figure 7 displays a partial schematic of the water flow test setup. The water test setup included a pressure measurement upstream of the needle valve along with a skin temperature measurement upstream of the needle valve which was representative of the demineralized water temperature.

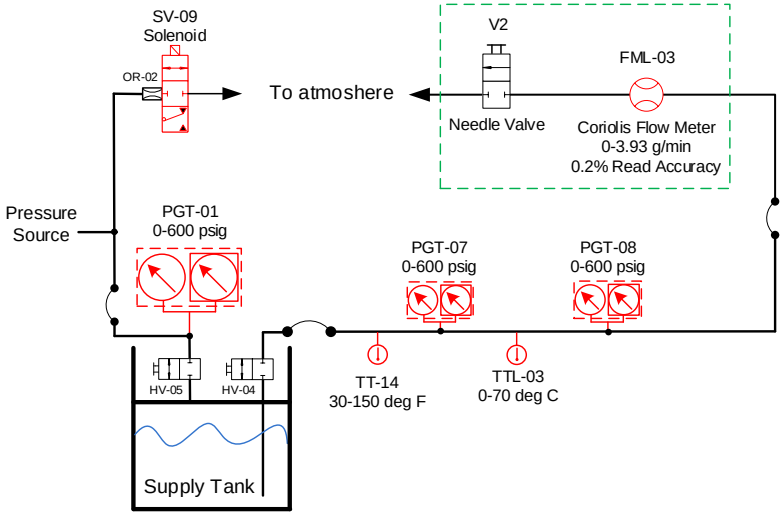


Fig. 7 Schematic of Water leak flow test setup.

B. GHe Leak Flow Test Setup

A partial schematic of the GHe leak flow test setup is presented in **Fig. 8**. The helium test setup included a pressure measurement upstream of the needle valve and a temperature probe measurement downstream of the needle valve.

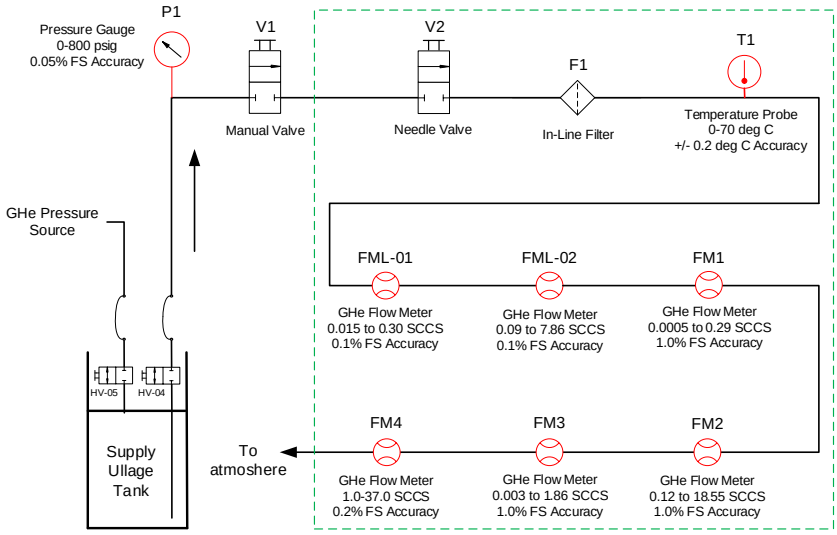


Fig. 8 Schematic of GHe leak flow test setup.

A set of six helium flow meters (FML-01, FML-02, FM1, FM2, FM3, and FM4) covering a few orders of magnitude of GHe flow rates from 0.0005 to 37.0 sccs (**Fig. 9**), which enabled an adequate correlation with the liquid Coriolis flow meter.

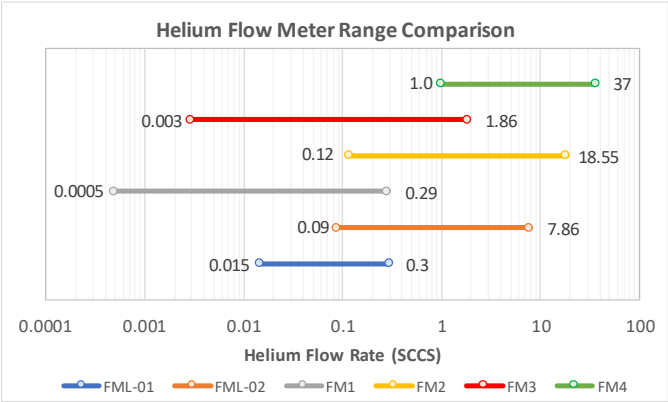


Fig. 9 Helium flow rate range for the six flow meters (within accuracy requirements).

C. Needle Valve Modification

After the flow meters were installed and testing commenced, the data still showed unacceptable repeatability. The leak rate was being set visually via an etched mark on the needle valve Vernier caliper. It was determined that this manual setting of the valve was contributing to the repeatability issue. The valve handle was therefore disassembled, and new caliper dial mechanisms were installed as shown in **Fig. 10 and Fig. 11** for the water flow setup and the GHe flow test setup, respectively. This new rigid dial allowed for the setting of the valve to be consistent for each run since the dial physically impacted the clip handle at each location. Provided the clips were not moved, the valve needle could be placed in nearly the same exact position every time.

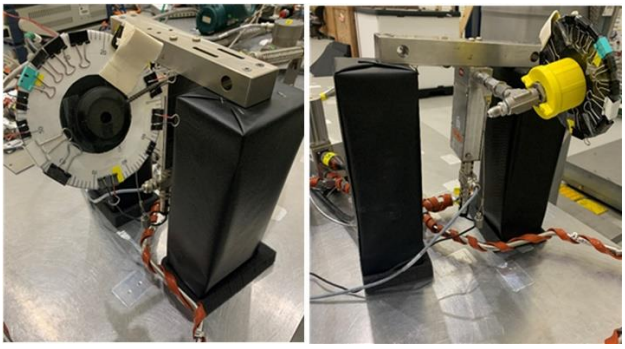


Fig. 10 Needle valve custom caliper dial mechanism and Coriolis flow meter in water flow setup.

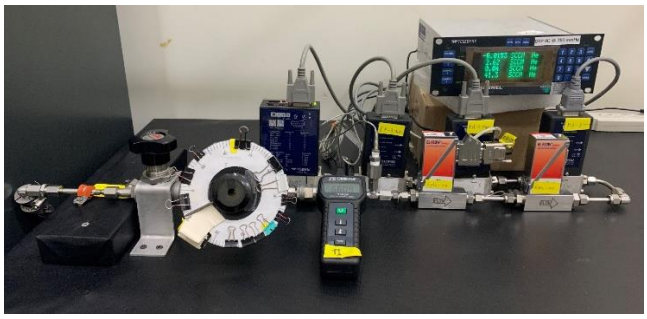


Fig. 11 Needle valve custom caliper dial mechanism in helium flow setup.

The control system was connected to the FML-01 and FML-02 helium flow meters. The control system enabled digital recording of all the data except for P1, T1, FM1, FM2, FM3, and FM4. These six instruments were manually recorded for each data point.

It took a few trial runs to establish the liquid test process since specific timing was required to obtain repeatable results with the Coriolis flow meter. The Coriolis flow meter exhibits a feature that it asymptotically approaches its reading over a relatively long period of time, specifically for the lower flow rates. With the same timing used for each run, the data was repeatable.

IV. Results and Discussion

A. Helium Leak Tests

After a few trial test runs were performed in the helium leak test setup, a process was established which showed very good promise for repeatability of test results. It was decided to perform the test at three separate pressures (280, 300, and 320 psig) to establish the sensitivity of system pressure to the leak correlation. The helium and demineralized water temperature were fairly comparable to the test facility room temperature, and typically varied between 64 and 71 degrees F. Once the data falling outside of the calibrated range of each flow meter was excluded, it is found that there is a consistent trend across all the flow meters (a single continuous curve). **Figs. 12a-12c** shows a summary of the full dataset from the six helium flow meters for the 280 psig, 300 psig and 320 psig test runs, respectively, indicating the dependence of helium leak rate as a function of the needle valve position. Also, the standard deviation for each data point was relatively low for the repeated runs as indicated by the error bars on the figures.

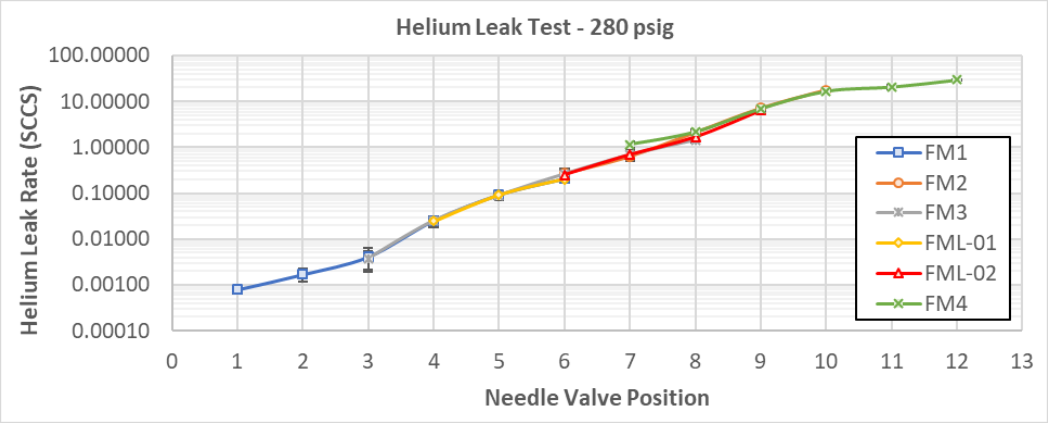


Figure 12a. Helium leak test results (280 psig supply pressure).

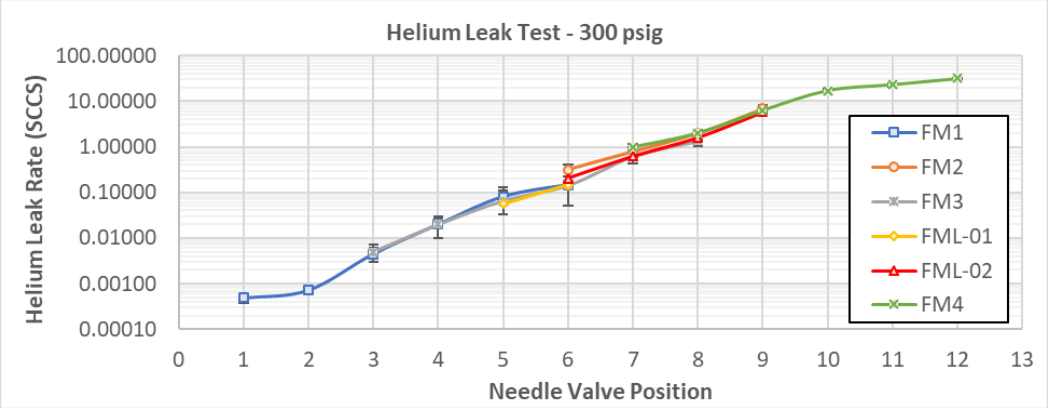


Fig. 12b Helium Leak Test Results (300 psig supply pressure).

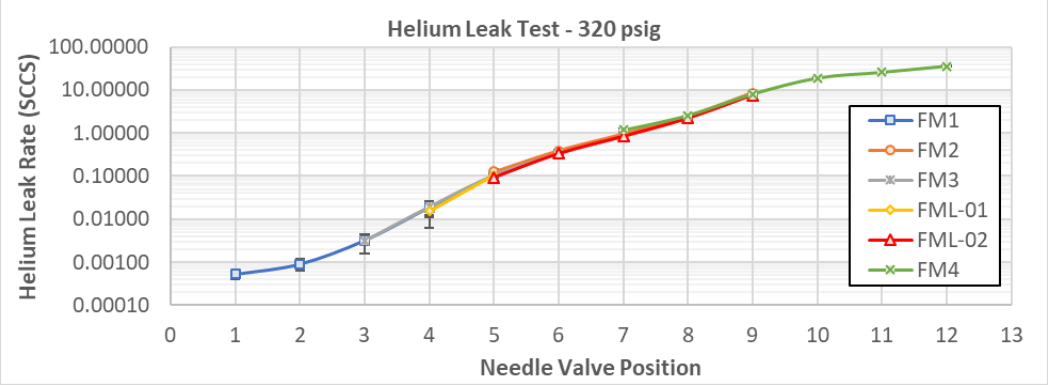


Fig. 12c Helium leak test results (320 psig supply pressure).

B. Water FlowTests

As with the helium flow test runs, the first few demineralized water flow tests were considered as trial runs and the data was discarded. Formal testing began on the fifth water test run once the timing of each flow rate to reach quasi-steady state was well understood at each needle valve position. The five lower flow rate needle valve positions

required a longer hold time before the data point was taken (see **Table 1**). This slow decay in flow rate over time was also seen in in the data of Blair and Senear (1968).

Table 1. Data collection timing utilized for water flow testing.

Needle Valve Position	Time (min:sec)	Approx. Flow Rate (grams/min)
1, 2, 3, 4, 5	5:00	0.001 to 0.05
6	4:00	0.1
7, 8, 9, 10, 11, 12	2:00	0.2 to 3.9

Utilizing the timing summarized in Table , the demineralized water flow test data was quite repeatable and had very little variation from one test run to another as shown in **Fig. 13**. The error bars signifying the standard deviations are barely visible for most of the data points. It is also shown that the supply pressure did not exert appreciable variation in the valve position-water flow rate curve. For a given needle valve position, the water flow rate slightly increases as the supply pressure is increased (as we would expect since the downstream pressure is held at the ambient).

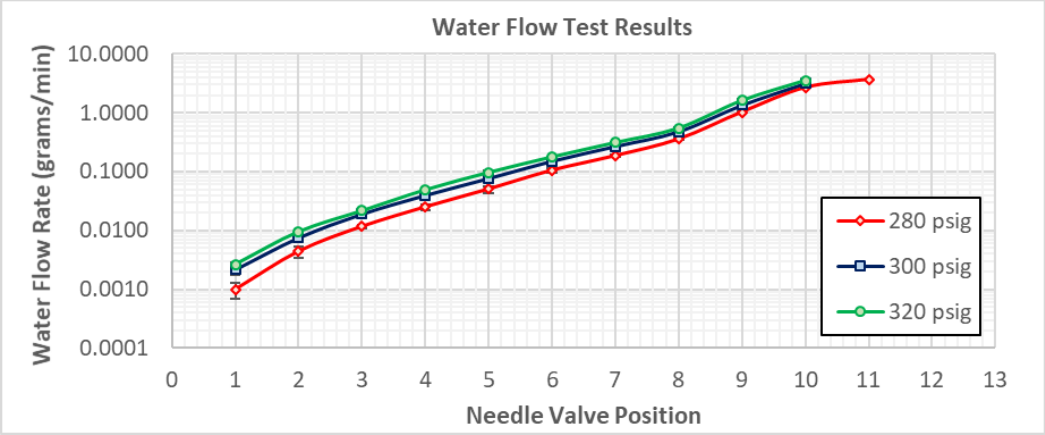


Figure 13. Water flow test results at 280, 300, and 320 psig supply pressure.

C. Comparison of Present Test Data with the Data of Blair and Senear

The present data shown in **Figs**. 12 and 13 for the helium and demineralized water flow, respectively, were combined to arrive at the direct correlation between helium and water leak rates at the same needle valve position, i.e., the same leak orifice geometry. This data correlation is shown in **Fig. 14**. Since the needle positions are repeatable using the modified caliper dial and clips, it is assumed that the setting on the needle valve was the same between the tests performed with the helium and water test setups. On a log-log scale a nearly linear dependence (of water flow rate on helium flow rate) is seen except at the lower flow rates (below about $5x10^{-3}$ sccs GHe) where a definite non-linear dependence is noted. On the other hand, the helium and distilled water test data of Blair and Senear[1] showed a linear trend over a wider range of GHe flow rates. This linear trend in a log-log plot was also revealed in the present analysis, except in the low helium flow rate limit tested.

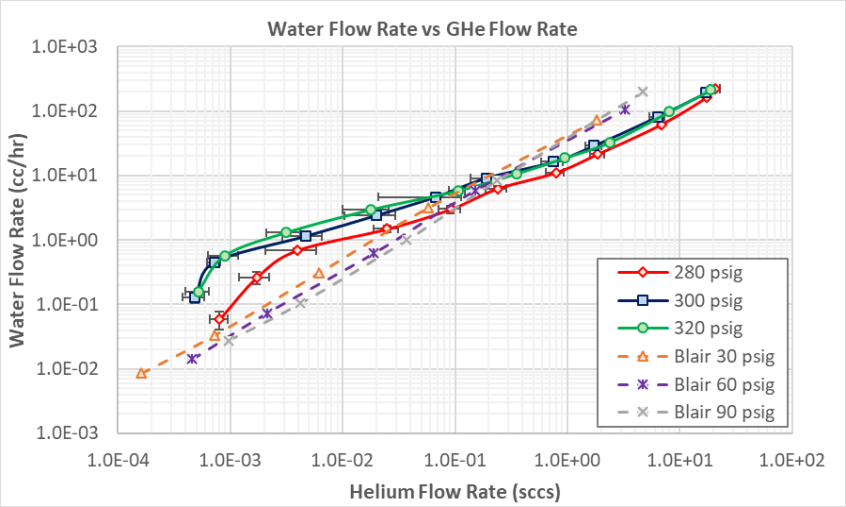


Fig. 14 Helium and water flow rate correlation at various supply pressures.

The differences between the present test data and Blair and Senear data may be partly attributable to differences in testing methods. The dissimilar fluid properties of distilled and demineralized water may also introduce some minor differences. It should be noted, however, that the system pressure levels in Blair and Senear's data, as shown in this plot, are substantially lower than those in the present tests. At a given GHe flow rate, the Blair and Senear data (as well as the present theory) show that water mass flow rates decrease with increased upstream system (supply) pressures. This is to be expected on physical grounds, since for a given (arbitrary) leak size, both the GHe flow rate and the water flow rate are expected to increase with an increase in system pressure. On the other hand, the present data displays an opposite trend. The cause of this discrepancy remains to be explained and resolved. A detailed examination of the present data revealed that testing variables during the GHe flow rate measurement at 280 psig is likely causing the discrepancy.

Although both the present data and Blair and Senear's data are within an order of magnitude, the nonlinear nature of the present data at reduced GHe flow rate warrants further investigation with possible improvement in the present measurement method.

D. Comparison of Theory with ExistingTest Data

Comparison with Test data of Blair and Senear[1]

Figure 15 displays a comparison of present theory (based on Eqs. 1 and 9) with the data of Blair and Senear[1] for water vs. GHe leak rates for three different supply pressures (30, 60 and 90 psig). The results show that the theory predicts the data reasonably well for GHe flow rate in the range of 0.001 to 1 sccs.

However, outside this range (GHe flow rate below 0.001 sccs and greater than 1 sccs), there is considerable deviation between the theory and the data. It appears that there is a possibility for further improvement of the theory on the gas side for low GHe flow rates, and on the liquid side for high GHe flow rate. At high liquid flow rates, it is possible that the liquid flow could be unsteady and turbulent in the highly complex and tortuous leak path.

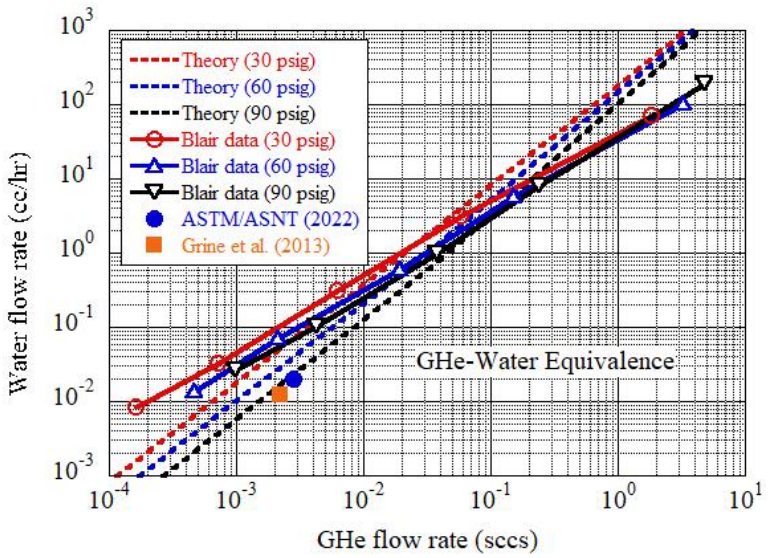


Fig. 15 Comparison of present theory with experimental data of Blair and Senear[1] for water and GHe flow rate equivalence.

Additional Comparisons

According to Leakage Testing Handbook[13], 1 scch (2.8×10^{-4} sccs) of GHe is equivalent to 0.0202 cc/hr of water (independent of system pressure), while the present theory shows that a leak rate of 1 scch of GHe is equivalent to 0.015 cc/hr of water. In the experiments of Grine et al.[14], at an internal gas pressure of about 90 psig (and a gasket pressure of 885 psig, holding the o-ring between the two raised face of the flanges), a GHe leak rate of 2.2×10^{-3} sccs results in an equivalent water leak rate of 0.0126 cc/hr. The present theory, on the other hand, gives an equivalent water leak rate of 0.05 cc/hr, thus providing an order of magnitude comparison. Fig. 15 reveals that the data from both the Leakage Testing Handbook (ASTM/ASNT)[13] and Grine et al.[14] agree closely with the present prediction (corresponding to 90 psig supply). Also, in a recent study concerning Mars sample sealing system by Redmond et al.[15], it was shown that a GHe leak rate of 10^{-8} sccs over a 20-year period is equivalent to a water leak of 3 mg. On the other hand, the present predictions show that the corresponding water leak of 0.72 mg, providing an order of magnitude comparison.

V. Conclusions

Data for helium leak rates and equivalent water leak rates were obtained in ground tests for a given leak size for various supply pressures. The correspondence (equivalence) between helium leak rates and water leak rates for the same leak size was established by a combination of experimental data for GHe and water flow tests, theoretical analysis, and scaling laws. The scaled data from Blair and Senear[1] showed an order of magnitude agreement with the present data for water-GHe equivalence in the range of flow rates tested. The present analysis, based on Knudsen number dependence in the slip flow regime for the low GHe flow rates (as opposed to continuum assumption), seems to agree reasonably with the Blair and Senear test data.

With the knowledge of gas-to-liquid leak rate correspondence and the helium leak test data received during the flight operations, the mission operators will be able to quantify the risk of any residual propellant leakage following the system priming and/or during on-orbit propellant transfer. This process requires the selection of applicable analytical modeling techniques for liquid leak rates based on the range of measured helium leak rates. One-size-fits-all analytical model does not likely work for the entire range of measured GHe leak rates.

Acknowledgments

This work was funded by the NASA's Exploration and In-Space Services (NExIS) Division, Goddard Space Flight Center in cooperation with NASA Kennedy Space Center.

References

[1]Blair, A.W and Senear, A.E., "Measurement and Correlation of Helium and Fluid Leak Rates." The Boeing Company. Prepared for NASA Manned Spacecraft Center, Houston, TX (Contract NASw-1650. D2-114258-1), July 29, 1968.

[2]Cincinnati Test Systems, How to establish an acceptable leak rate, Application Bulletin #120, October 2014.

[3]Shapiro, A.H., The Dynamics and Thermodynamics of Compressible Fluid Flow, Volume 1, John-Wiley, New York, 1953.

[4]Kandula, M., Nufer, M., Felt, A.M., Aranyos, T.J., Webster, G.K., and Coll, G.T., Compressibiloity, Reynolds number and thermal effects in pressure-decay based leak detection systems, AIAA-2019-3437, AIAA Fluid Dynamics Cnference, Dallas, Texas, June 17-21, 2019.

[5]Bragg, S.L., Effects of compressibility on the discharge coefficient of orifices and convergent nozzles, *Journal of Mechanical Engineering Science*, Vol. 2, No. 1, 1960.

[6]Wang, X., Kruis, F.E., and McMurray, P.H., Aerodynamic focusing of nanoparticles: I. Guidelines for designing aerodynamic lenses for nanoparticles, *Aerosol Science and Technology*, Vol. 39, pp. 621-623, 2005.

[7]Tuve, G.L., and Sprenkel, R.E., Orifice discharge coefficients for viscous liquids, *Instruments*, Vol. 6, pp. 201-206, 1933.

[8]Vincenti, W.G., and Kruger, C.H., Introduction to Physical Gas Dynamics, Krieger Publishing Company, Malabar, Florida, 1986.

[9]Agrawal, A., A comprehensive review on gas flow in microchannels, International Journal of Micro-Nano Scale Transport, Vol. 2, No. 1, 2011.

[10]Dongari, N., Agrawal, A., and Agarwal, A., Analytical solution of gaseous slip flow in long microchannels, International Journal of Heat and Mass Transfer, Vol. 50, pp., 3411-3421, 2007.

[11]Shames, I.H., Mechanics of Fluids, 2nd ed., McGraw-Hill, New York, 1982.

[12]Hrnjak, P., and Tu, X., Single phase pressure drop in microchannels, International Journal of Heat and Fluid Flow, Vol. 28, pp. 2-14, 2007.

[13]Leakage Testing Handbook, ASTM E1316-22 and ASNT Nondestructive Testing Handbook, 4th ed., Vol. 2, Leak Testing, 2022.

[14]Grine, L., and Bioutid, A-K., Analytical and experimental studies of liquid and gas leaks through micro- and nano-porous gaskets, Materials Sciences and Applications, Vol. 4, pp. 32-42, 2013.

[15]Redmond, M., Berisford, D., and Bhandari, P., Water and helium leak rate requirements for a mars ample sealing system, ICES-2015-23, 45th International Conference on Environmental Systems, Bellevue, Washington, July 12-16, 2015.